

Research Paper

Physically reliable 3D styled shape generation via structure-aware topology optimization in unified latent space

Haroon Ijaz, Xuwei Wang, Wei Chen, Hai Lin, Ming Li *

State Key Laboratory of CAD&CG, Zhejiang University, Hangzhou, 310027, China

ARTICLE INFO

Keywords:

Generative design
3D shape creation
Topology optimization
Variational autoencoder
Finite element analysis
Global convergent MMA

ABSTRACT

We propose a novel approach to structure-aware topology optimization (SATO) to generate physically plausible multi-component structures with diverse stylistic variations. Traditional TO methods often operate within a discrete voxel-defined design space, overlooking the underlying structure-aware, which limits their ability to accommodate stylistic design preferences. Our approach leverages variational autoencoders (VAEs) to encode both geometries and corresponding structures into a unified latent space, capturing part arrangement features. The design target is carefully formulated as a topology optimization problem taking the VAE code as design variables under physical constraints, and solved numerically via analyzing the associated sensitivity with respect to the VAE variables. Our numerical examples demonstrate the ability to generate lightweight structures that balance geometric plausibility and structural performance with much enhanced stiffness that outperforms existing generative techniques. The method also enables the generation of diverse and reliable designs, maintaining structural integrity throughout, via a direct smooth interpolation between the optimized designs. The findings highlight the potential of our approach to bridge the gap between generative design and physics-based optimization by incorporating deep learning techniques.

1. Introduction

Generative design is a computational approach that explores a wide range of design options within predefined constraints, inspiring innovative solutions beyond conventional ideas. Recently, deep generative models (DGMs), particularly variational autoencoders (VAEs), have significantly advanced 3D shape generation by capturing complex geometric details, making them crucial in fields like architecture, aerospace, and automotive engineering [1]. In parallel, topology optimization (TO) has established itself as a key method for creating novel shape topologies under physical constraints [2], or manufacturing constraints [3]. Traditional TO methods typically discretize the entire design space, assigning material density to each element in the grid to optimize goals such as structural compliance.

However, these traditional TO methods mainly work within a discrete voxel-defined design space and often overlook structure-aware properties, such as design styles or the arrangement of components [4–6]. This limitation restricts their ability to produce designs that are not only functionally robust but also visually appealing, especially in applications where styles are as important as structural integrity. While state-of-the-art methods have focused on visual appearance only [7–9], they often fail to generate physically reliable 3D shapes. For instance, the SDMNet model [10] produces a chair with an unnecessarily heavy

or unsteady structure under poorly designed loading conditions, as illustrated in Fig. 2.

To bridge the gap between generative design and TO, we introduce a novel TO method called structure-aware topology optimization (SATO) incorporating structure-aware principles. Our approach leverages the latent space of a VAE [11], which encodes geometric shape and part arrangement, into a unified representation. The unified representation provides the geometry as a collection of separate components and the structure as pairs of bounding boxes, which enables the generation of diverse, physically reliable structures that satisfy both mechanical performance criteria and stylistic preferences. An overview of SATO is shown in Fig. 1.

The main technical challenges involve a clear mathematical problem formulation and an efficient, reliable numerical approach to finding solutions that satisfy geometric and physical constraints. Under physical constraints, we formulate the problem as a TO problem, taking the design variables from a unified VAE space that encodes both the part geometry and their inter-relation uniformly. This latent space naturally enables the generation of structurally reliable designs while maintaining component interdependencies. To obtain the solution, the sensitivity of the generated structure's properties with respect to (w.r.t)

* Corresponding author.

E-mail address: liming@cad.zju.edu.cn (M. Li).

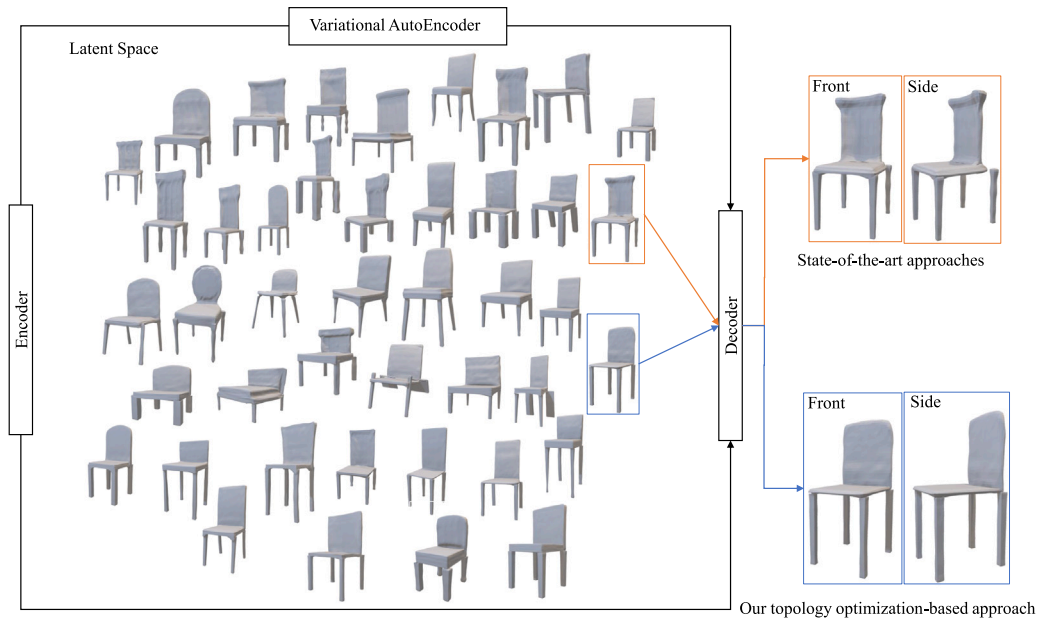


Fig. 1. Overview of our SATO based approach for generating physically reliable 3D shapes. Unlike methods that prioritize visual appearance over functionality, our approach integrates stylistics and different components, ensuring the selection of lightweight, structurally robust, and optimized shapes for efficient load-bearing.

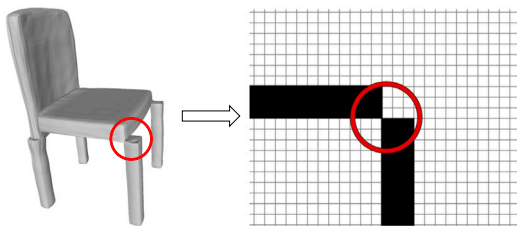


Fig. 2. Optimized chair using a traditional optimization method. The chair has poorly designed connectivity areas between components, leading to inadequate load distribution and an unnecessarily heavy structure.

the VAE design parameters is derived analytically by leveraging the automatic differentiation (AD) of the VAE network.

Our main contributions are as follows:

1. A structure-aware TO approach (SATO) generates various physically reliable and geometrically plausible structures in various styles, via encoding both local geometry and its structure in a unified latent space. This approach minimizes structural compliance while preserving geometric features.
2. A numerical approach tackles the SATO problem by deriving analytically the associated sensitivity w.r.t. the VAE design variables by leveraging the problem’s mathematical formulation and the AD of the VAE network.
3. A direct approach generates versatile physically sound shapes, which much overcomes the unstable and overly dense shapes generated from previous learning approaches, achieved via interpolation between the source and target SATO shapes, owing to their uniform VAE representations.
4. Performance of the SATO is tested via various numerical examples across multiple volume fractions (0.3–0.7), loading conditions, and different case studies, demonstrating its ability to produce different styled physically optimized shapes.

Additionally, to facilitate understanding, the main terminologies used in this work are listed in Table 1.

The remaining part is arranged as follows. Section 2 reviews the existing methods. Section 3 formulates the SATO problem, followed by the details and implementation respectively in Sections 4 and 5. Section 6 presents and evaluates the numerical results, and Section 7 concludes the study.

2. Related work

2.1. Learning-based 3D shape generation

Recent advances in 3D shape generation have explored diverse input modalities, including images [12,13], point clouds [14–16], voxels [7,17–19], meshes [20,21], signed distance functions (SDF) [12,22], latent vectors [23,24], neural fields [25,26], text-to-shape [27–29], and image-to-shape [12,13].

Voxel representations, popular for their regular structure and compatibility with 3D CNNs, simplify FEA and support efficient TO algorithms. For example, Wu et al. [8] combine voxel-based shape generation with part segmentation, and Wang et al. [18] incorporate physical constraints within voxel-based VAEs. Meshes offer finer surface details and are essential for precise physical simulations. SDM-Net [10] generates mesh-based shapes with semantic part awareness, while CLIP-Forge [30] enables text-guided mesh generation.

Deep generative models (DGMs) have transformed 3D shape generation by learning complex shape distributions from large datasets. In these studies, VAEs are often preferred over candidates for their stability and ease of shape manipulation and interpolation [31,32]. For example, DeepSDF [33] uses a VAE to learn a continuous signed distance function for 3D shapes, enabling the generation of high-fidelity models, while Zhang et al. [23] demonstrate VAE-based shape generation with controllable category-specific attributes.

These works use different approaches to produce 3D shapes. However, these works often prioritize appearance over structural integrity and hence none of them address the challenges of generating physically reliable shapes. Despite yielding visually appealing shapes, these methods often fail to ensure physical reliability, highlighting the persistent challenge of balancing visual quality with structural integrity.

Table 1
Main terms.

Term	Full meaning
SATO	Structure-Aware Topology Optimization
TO	Topology Optimization
FEA	Finite Element Analysis
FEM	Finite Element Method
MMA	Method of Moving Asymptotes
GCMMA	Global Convergent MMA
AD	Automatic Differentiation
DGM	Deep Generative Models
VAE	Variational Autoencoder
CNN	Convolutional Neural Network
PINN	Physics-Informed Neural Network
nelx	The number of elements in the x direction
nely	The number of elements in the y direction
nelz	The number of elements in the z direction
volfrac	Volume Fraction
penal	Penalization Power
rmin	Filter Radius
SDF	Signed Distance Function
MMC	Moving Morphable Components
w.r.t	with respect to
Stylistic	Unique variations in structural and geometric features of shapes.
Part Arrangement	Spatial organization and positioning of structural components.
Geometric Plausibility	Functional validity of part connections and arrangements.
Shape Semantic	Functional or meaningful significance of a shape's design.
Component/ Part	Structural elements of a design (used interchangeably).
Visual Appearance	Overall look and aesthetic appeal of generated structures.

2.2. TO-based 3D shape generation

Topology optimization aims to automatically generate a 3D shape for optimal physical performance [2] and often operates within a discretized design domain. Incorporating high-level design semantics during the optimization is one of its high-demand targets, enabling explicit control of various design or manufacturing constraints [34–38]. In particular, the Moving Morphable Component (MMC) approach [39] has emerged as one of the pioneering methods by utilizing explicitly defined morphable components that can move, deform, overlap, and disappear to create optimized designs. This approach effectively addresses low-level semantics [40,41] but struggles with high-level semantics like style and part arrangement, limiting their ability to generate varying styles according to design preferences.

Integrating machine learning (ML) into TO has accelerated and diversified TO methods, enabling more customized design generation [42]. Zhang et al. [43] introduced an ML-enhanced approach to structural TO that incorporates human design preferences, aligning the optimization process with designer intentions. ML-driven TO approaches often employ neural networks to predict optimized material distributions under specific loading and boundary conditions [44, 45]. For instance, Jeong et al. [46] developed CPINNTO, a structural optimization framework based on physics-informed neural networks (PINNs). In 3D design, Zhang et al. [47] presented a method for generating optimized glider shapes using a VAE trained on an extensive 3D structure dataset [48]. Furthermore, style transfer with 2D image data has been applied to VAEs [49], ensuring that designs generated in latent space maintain aesthetic alignment with original shapes while meeting structural requirements.

While these VAE and ML-based techniques have advanced TO, these methods often struggle with the complexities of multi-component systems, where interaction and connectivity between components are crucial to structural integrity.

3. Overview and problem formulation

We aim to generate various physically reliable and structure-aware aesthetic structures in different styles. Traditional TO methods have struggled to incorporate stylistic elements, such as the arrangement of components and style consideration, into the design process. We address this by utilizing a VAE to jointly encode part geometry and their relative locations, forming the basis of a novel topology optimization problem. The VAE helps capture the inter-dependencies between geometric and structure-aware features and optimizes simultaneously the design's part geometry, relative locations, and overall physical properties.

3.1. VAE architecture and structure encoding

VAE is a generative model that learns a probabilistic mapping from a latent space \mathbf{z} to the data space \mathbf{x} . The VAE consists of three main components: the encoder, the latent space, and the decoder [11].

The encoder $q_\phi(\mathbf{z}|\mathbf{x})$ maps the input \mathbf{x} to a latent space \mathbf{z} , where ϕ represents the parameters of the encoder. It outputs the mean μ and the standard deviation σ of a Gaussian distribution:

$$q_\phi(\mathbf{z}|\mathbf{x}) = \mathcal{N}(\mathbf{z}; \mu(\mathbf{x}), \sigma^2(\mathbf{x})). \quad (1)$$

From this Gaussian distribution, a latent vector \mathbf{z} is sampled:

$$\mathbf{z} = \mu(\mathbf{x}) + \sigma(\mathbf{x}) \odot \epsilon, \quad (2)$$

where $\epsilon \sim \mathcal{N}(\mathbf{0}, \mathbf{I})$ is a standard normal distribution, and \odot denotes element-wise multiplication.

The decoder $p_\theta(\rho|\mathbf{z})$ maps the \mathbf{z} back to the data space, where θ represents the parameters of the decoder. The decoder reconstructs the input \mathbf{x} as output ρ :

$$p_\theta(\rho|\mathbf{z}) = \rho(\mathbf{z}). \quad (3)$$

The VAE is trained to maximize the evidence lower bound (ELBO), which combines the reconstruction loss and the Kullback–Leibler (KL) divergence:

$$\mathcal{L}(\theta, \phi; \mathbf{x}) = \mathbb{E}_{q_\phi(\mathbf{z}|\mathbf{x})}[\log p_\theta(\rho|\mathbf{z})] - \text{KL}(q_\phi(\mathbf{z}|\mathbf{x})||p(\mathbf{z})), \quad (4)$$

where $p(\mathbf{z}) = \mathcal{N}(\mathbf{z}; \mathbf{0}, \mathbf{I})$ is the prior distribution over the latent space.

3.2. Problem formulation

Traditional TO operates on discretized single-body design spaces and requires even hundreds of millions of DOFs (Degrees of Freedom). Its direct application meets two main challenges: (1) multi-component design requires simultaneous optimization of both component-level geometry and spatial configurations within a continuous design space; (2) TO is computationally expensive and even practically unfeasible.

We tackle these challenges by performing design optimization within a VAE latent space, which enables us to capture important geometric features while maintaining the expressiveness necessary for structural design. Instead of directly optimizing the physical parameters of the design, we focus on optimizing the latent variables \mathbf{z} .

Based on the above considerations, the problem of structure-aware topology optimization (SATO), in a classic form of compliance minimization, is formulated as follows,

$$\begin{aligned} &\text{find } \mathbf{z} \sim \mathcal{N}(\mu_{\mathbf{z}}, \sigma_{\mathbf{z}}^2) \\ &\text{min } c(\rho) = \mathbf{U}^T \mathbf{K} \mathbf{U} \\ &\text{s.t. } g(\rho) = \frac{V(\rho)}{V_0} - V_f \leq 0 \\ &\quad \mathbf{K} \mathbf{U} = \mathbf{F} \\ &\quad 0 \leq \rho_i \leq 1, \quad i = 1, 2, \dots, N \\ &\quad \rho = \text{Dec}(\mathbf{z}), \quad \mathbf{z} \sim \mathcal{N}(\mu, \sigma^2) \end{aligned} \quad (5)$$

where c is the compliance, \mathbf{U} is the global displacement vector, \mathbf{K} is the global stiffness matrix, N is the number of elements in the discrete design domain, \mathbf{u}_i is the element displacement vector, \mathbf{k}_0 is the element stiffness matrix for an element with fully distributed solid material, and N is the number of finite elements. The volume fraction constraint is given by $g(\rho)$ where $V(\rho)$ and V_0 are respectively the material volume and the design domain volume, V_f is the pre-defined volume fraction, \mathbf{F} is the global force vector, \mathbf{z} is the vector of design variables (relative densities), E_i is Young's modulus of element ρ_i .

To handle the non-linearity and complexity of the optimization problem, we adopt the Global Convergent Method of Moving Asymptotes (GCMMA) [50], an advanced version of the traditional Method of Moving Asymptotes (MMA). GCMMA outperforms MMA by better handling nonlinear and coupled constraints, allowing faster convergence in large-scale structural optimization. It is particularly effective for nonlinear optimization problems with both inequality constraints and complementarity constraints, making it well suited for structural optimization tasks like designing a multi-component structure.

In technically resolving the above issues, we propose a hybrid method for computing gradients in the latent space combining analytical derivations and automatic differentiation (AD). GCMMA uses these gradients to update the design variables efficiently and ensure faster convergence during the optimization process. The integration of GCMMA optimization with hybrid gradient computation significantly enhances the performance and accuracy of the optimization process, particularly for complex, multi-part structures. This combination leverages the strengths of both approaches: GCMMA provides robust convergence properties, while hybrid gradient computation ensures efficient and precise gradient estimation, even for intricate geometries.

To the best of our knowledge, this specific combination has not been explored in prior studies. While GCMMA and hybrid gradient methods have been investigated independently, their synergistic application to optimize complex, multi-part structures represents a novel contribution to the field. This approach addresses key challenges in TO, such as handling non-linear constraints and improving computational efficiency, which are critical for achieving high-quality results in practical applications.

4. Methodology

Our novel framework is illustrated in Algorithm 1. It merges the VAE-based 3D geometric shape generation and the TO process, ensuring the creation of reliable structures. Detailed methodologies for VAE to encode the component-based structure and the numerical approach to solving the SATO problem in Eq. (5) are presented below.

4.1. Geometric 3D shape generation and encoding

Our particular interest is in generating novel topology-optimized 3D shapes by traversing the latent space. The VAE must capture both geometric features and the structural patterns from the TO pipeline.

We formulate a VAE to learn the joint distribution of geometry and structural features. This work adopts GRUs (Gated Recurrent Units), a type of Recurrent Neural Network (RNN), in the VAE architecture because they effectively model sequential dependencies and relationships between parts in 3D shapes. Unlike simpler methods like fully connected layers, GRUs can capture complex, long-range dependencies in both geometry and structure, which is crucial for generating plausible shapes. GRU has fewer gates but enables storing and filtering information with its internal memory. This alleviates the gradient vanishing problem during the network training. Furthermore, GRU has fewer learnable parameters, thereby achieving greater flexibility in a more principled training framework [51]. This makes GRUs well-suited

Algorithm 1: Algorithm for structure-aware topology optimization (SATO)

Input: nelx, nely, nelz, load size, load location, volfrac, boundary conditions, penal, rmin, VAE, initial latent vector, initial decoded density, $\frac{\partial \rho}{\partial \mathbf{z}}$

Output: Optimized latent vector \mathbf{z} , final physically reliable density distribution ρ

- 1 Construct a VAE;
- 2 Generate initial density from latent vector \mathbf{z} using Eq. (2);
- 3 Initialize optimization parameters;
- 4 Discretize decoded density ρ into voxel grid Fig 3;
- 5 **while not converged do**
- 6 Compute element stiffness matrices $k_i(\rho_i)$ using Eq. (14);
- 7 Assemble global stiffness matrix $K(\rho)$ using Eq. (16);
- 8 Solve for nodal displacements $U(\rho)$ using Eq. (17);
- 9 Compute compliance $c(\rho) = U(\rho)^T K(\rho) U(\rho)$;
- 10 Compute compliance sensitivity w.r.t. densities $\frac{\partial c(\rho)}{\partial \rho}$ using Eq. (18);
- 11 Compute density sensitivity w.r.t. latent vector $\frac{\partial \rho}{\partial \mathbf{z}}$ using Eq. (20);
- 12 Update latent vector using GCMMA optimization [50] ;
- 13 Generate new density using updated latent vector;

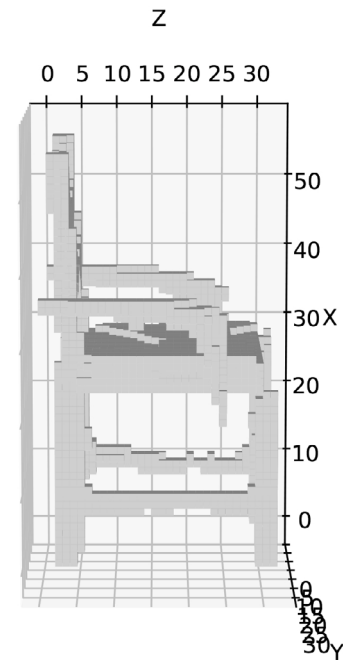


Fig. 3. A decoded mesh before processing through SATO pipeline.

for the joint analysis of geometry and structure in the VAE. The encoder processes two types of input features, respectively of part geometry,

$$h_g = G_{enc}^g(H_g), \quad H_g = h_i | i = 1, \dots, k \quad (6)$$

where H_g represents the sequence of geometry features for k components and G is GRU, and of the relative arrangement of parts,

$$h_s = G_{enc}^s(H_s), \quad H_s = h_{i,j} | i = 1, \dots, k, j \geq i \quad (7)$$

where H_s encodes structural relationships between components.

We combine the geometry vector in Eq. (6) and structure vector in Eq. (7) using another GRU with a part mask (c), which indicates the

presence or absence of each part in the shape. The part mask ensures that the model can handle shapes with varying numbers of parts. This GRU (G_v^c) fuses the geometry and structure features into a single joint feature (h_v) using the following equation:

$$h_v = G_v^c(f([h_g, c]), f([h_s, c])) \quad (8)$$

where $f([h_g, c])$ and $f([h_s, c])$ are fully connected layers that combine the geometry and structure features respectively with the part mask. The joint feature (h_v) is then passed through a fully connected layer to produce two vectors μ and σ to encode the latent space representing both geometry and structure, as follows:

$$\mathbf{z} = \mu + \sigma \mathbf{n} \quad (9)$$

where μ (mean), σ (variance) define the learned distribution parameters and \mathbf{n} is a random noise vector. More details are referred to [8].

In SATO, the VAE's latent space, defined by the μ and σ vectors, encodes essential geometric and structural relationships among parts. This latent representation enables the model to generate diverse, topology-optimized designs. Sampling from this space allows flexible exploration within the TO framework, supporting structural integrity and adaptable design variations, which is crucial for developing complex and optimized multi-component 3D structures.

The simulation and optimization of the VAE-represented structure are outlined in detail below.

4.2. Simulation aspects

The physical properties of the structure, such as stiffness and compliance, are computed using FEA. This allows us to evaluate the structural performance for each potential design, even in the latent space, by translating geometric parameters into physical behavior through the FEA.

We sample an initial 3D shape from the latent space mentioned in Eq. (9) (see Fig. 3). Following traditional topology optimization, our approach modifies these discrete values into continuous densities between 0 and 1, where values remain close to 0 but never actually reach zero, following

$$E_i(\rho_i) = E_{min} + \rho_i^p (E_0 - E_{min}), \quad (10)$$

where p is the penalization power ($p > 1$), E_{min} is the elastic modulus of the void material, set as 0.001 to avoid singularity of the finite element stiffness matrix, E_0 is the Young's modulus of solid material.

Using the FEM, the elastic solid element stiffness matrix is computed as

$$\mathbf{k}_i(\rho_i) = \int_{-1}^{+1} \int_{-1}^{+1} \int_{-1}^{+1} \mathbf{B}^T \mathbf{C}_i(\rho_i) \mathbf{B} d\xi_1 d\xi_2 d\xi_3, \quad (11)$$

where ξ_e ($e = 1, \dots, 3$) are the natural coordinates. The strain-displacement matrix \mathbf{B} relates the strain ϵ and the nodal displacement \mathbf{u} ,

$$\epsilon = \mathbf{B}\mathbf{u}. \quad (12)$$

The \mathbf{C}_i denotes the elements constitutive matrix following the SIMP approach

$$\mathbf{C}_i(\rho_i) = E_i(\rho_i) \mathbf{C}^0, \quad (13)$$

where \mathbf{C}^0 is the constitutive matrix with unit Young's modulus. The element stiffness matrix can be further written as,

$$\mathbf{k}_i(\rho_i) = E_i(\rho_i) \mathbf{k}^0, \quad (14)$$

where,

$$\mathbf{k}^0 = \int_{-1}^{+1} \int_{-1}^{+1} \int_{-1}^{+1} \mathbf{B}^T \mathbf{C}^0 \mathbf{B} d\xi_1 d\xi_2 d\xi_3, \quad (15)$$

The global stiffness matrix \mathbf{K} is obtained by the assembly of element-level counterparts \mathbf{k}_i ,

$$\mathbf{K}(\rho) = \sum_{i=1}^N E_i(\rho_i) \mathbf{K}_i^0, \quad (16)$$

where \mathbf{K}_i^0 is the global version of \mathbf{k}_i ,

Finally, the nodal displacements vector $\mathbf{U}(\rho)$ is the solution of the equilibrium equation

$$\mathbf{K}(\rho) \mathbf{U}(\rho) = \mathbf{F} \quad (17)$$

where \mathbf{F} is the vector of nodal forces.

4.3. Optimization aspects

The SATO problem formulated in Eq. (5) is solved by using the GCMMA optimizer [50]. The sensitivities of both the design target and constraints w.r.t the VAE variables are derived analytically in combination with the AD mechanism of the VAE network.

Using the chain rule, we first derive the derivatives of $c(\rho)$ w.r.t the VAE design variable z_j ,

$$\frac{\partial c(\rho)}{\partial z_j} = \sum_{i=1}^N \frac{\partial c(\rho)}{\partial \rho_i} \frac{\partial \rho_i}{\partial z_j}, \quad (18)$$

where $\frac{\partial c}{\partial \rho_i}$ is the gradient of compliance with respect to the part ρ_i of the 3D output shape (ρ), and $\frac{\partial \rho_i}{\partial z_j}$ is the gradient of the 3D output shape w.r.t the latent space (\mathbf{z}).

Notice that the compliance $c(\rho)$, as our objective function, is defined as

$$c(\rho) = \mathbf{U}^T \mathbf{K}(\rho) \mathbf{U} = \sum_{i=1}^N E_i(\rho_i(\mathbf{z}_i)) \mathbf{u}_i^T \mathbf{k}_0 \mathbf{u}_i. \quad (19)$$

The derivative of $c(\rho)$ with respect to the density ρ_i can be derived based on the adjoint theory [52,53]

$$\frac{\partial c(\rho)}{\partial \rho_i} = -p \rho_i^{p-1} E_0 \mathbf{u}_i^T \mathbf{k}_0 \mathbf{u}_i. \quad (20)$$

The term $\frac{\partial \rho_i}{\partial z_j}$ represents the sensitivity of the material distribution ρ_i of part i w.r.t the design variable z_j . This derivative is computed using automatic differentiation (AD), a method that efficiently calculates derivatives by applying the chain rule to a sequence of elementary operations. AD avoids both the inaccuracies found in numerical differentiation and the complexity of symbolic differentiation. This makes it ideal for complex models where material properties ρ_i depend on nonlinear mappings of design variables.

Similarly, the derivative of the volume constraint $v(\rho)$ with respect to the design variable z_j is computed

$$\frac{\partial v(\rho)}{\partial z_j} = \sum_{i=1}^N \frac{\partial v(\rho)}{\partial \rho_i} \frac{\partial \rho_i}{\partial z_j}, \quad (21)$$

where the term $\frac{\partial v(\rho)}{\partial \rho_i}$ is simply the volume v_i of element i , as given by:

$$\frac{\partial v(\rho)}{\partial \rho_i} = v_i. \quad (22)$$

These equations allow us to compute the sensitivities required for updating the design variables \mathbf{z} during the topology optimization process, subject to the volume constraint and minimizing compliance (maximizing stiffness).

Once the gradients are computed and the design variables are updated, the latent variables \mathbf{z} are decoded back into the material distribution ρ and the corresponding geometry. This decoded representation is used to evaluate the structural performance (compliance) and to enforce the constraints (volume). The process repeats until convergence, where the material distribution and geometry are jointly optimized to minimize compliance while satisfying the volume constraint.

5. Implementation details on SAGNet

SATO builds on the proven SAGNet framework [8] for managing part-based relationships and their unified VAE encoding. The partition strategy for generating k parts is based on coarse segmentation with consistent part ordering, which reduces complexity. Pairwise relationships are encoded as 6D bounding boxes, effectively capturing spatial dependencies. This structured approach aligns well with our SATO framework by preserving part relationships and facilitating the learning of inter-relations critical for generating optimized and structurally sound designs. Additionally, The input to our framework consists of geometries and bounding boxes.

The input to SAGNet-based VAE comprises k parts, with each part having a corresponding geometry in voxel format and a bounding box. Key elements, such as datasets and architecture, are highlighted here for ease of explanation. More details are referred to [8].

5.1. Dataset

We follow the dataset that comes with the SAGNet shape dataset that includes geometries and bounding boxes for different classes such as chairs, guitars, lamps, motorbikes, and tenon-mortise joints. The class of tenon-mortise joints is synthesized to evaluate the necessity of joint analysis of geometry and structure which benefits our SATO work. The dataset includes 10,000 synthetic examples, such as tenon-mortise joints with eight connection modes, to highlight inter-relational geometry dependencies.

5.2. Architecture

The framework consists of a two-branch autoencoder aligned with voxel mesh outputs: the upper branch processes geometry, and the lower branch processes structure. The geometry branch contains five 3D convolutional layers in the encoder, accepting k ($32 \times 32 \times 32$) voxel maps as input. These layers down-sample the voxel maps by a factor of 16, followed by a fully connected layer that computes k 512D features.

Simultaneously, the structure branch employs a fully connected layer to process K pairs of bounding boxes, generating K 512D features. The encoder's outputs feed into two GRUs that capture part relationships for both geometry and structure. These GRUs use Geometry and Structure Attention components to exchange information, producing k and K 200D features for the 2-Way VAE. The decoder mirrors the encoder, using five 3D deconvolutional layers to reconstruct voxel maps and a fully connected layer to regress latent features to bounding boxes, yielding a unified latent space encompassing both shape geometry and structure.

6. Numerical results and evaluation

We have implemented our structure-aware TO framework SATO on a standard workstation equipped with an NVIDIA GeForce GTX 970. In the study, all design domains are assumed to consist of materials with a Poisson's ratio of $\nu = 0.3$, Young's modulus of $E_0 = 1$, and a minimum modulus $E_{\min} = 1 \times 10^{-9}$. The default values are set as penal=3 and rmin=1.3 (filter radius) for all examples. The load was imposed on the upper surface of the seat directed downwards opposite to the Y direction while opposite to the X direction for the backrest, and the leg parts touching the ground are fixed. BCs are set manually at the start of the GCMMA iteration and remain fixed throughout to ensure convergence. Binary voxels (0, 1) are converted to continuous densities ($\rho \in (0, 1)$) for gradient-based optimization, with the force vector (F) in Eq. (17) remaining constant to maintain structural continuity at BC regions. The concrete parameters for the examples are summarized in

Table 2. The optimization stopping criteria for problem in Eq. (5) is based on the traditional TO convergence criteria,

$$\|x_{\text{new}} - x\|_{\infty} \leq 0.01, \quad (23)$$

We employed a VAE model based on the work of SDMNet [10], augmented with an additional layer to calculate signed distance function (SDF) values, which are used for converting triangular meshes into voxel meshes for our FEA module. The SDF offers high accuracy and control by representing the shortest distance to an object's surface, ensuring precise voxelization.

We test and evaluate our method's ability to generate lightweight structures that optimize both visual appearance and structural integrity, specifically, physically reliable 3D shape generation in Section 6.1, style-driven 3D shape generation in Section 6.2, and volume-constrained shape generation in Section and 6.3.

6.1. Physically reliable shape generation

We first test the effectiveness of our method in generating physically reliable shapes and compare it with SAGNet and SDMNet. Two cases are conducted: direct shape generation in comparison with SAGNet [8] and SDMNet [10] in Section 6.1.1, and topology-preserving interpolation in the latent space in Section 6.1.2.

6.1.1. Comparative analysis

In this section, we conduct a comparative analysis with recent works, specifically SAGNet [8], to evaluate the effectiveness of SATO in producing structurally sound and geometrically plausible designs under varied conditions.

In this test, we selected four different initial structures (a, b, c, d) generated by SAGNet and assigned volume fractions of 45%, 40%, 35%, and 30% respectively. A vertical load of 40N was applied to the chair seat area. The results are shown in Fig. 4, where the generated designs from SAGNet are shown in the left column, and our SATO in the middle. The associated convergence curves of ours are also shown in the rightmost column; the iterations for each case were 72, 65, 79, and 81, respectively.

The comparison revealed a notable reduction in compliance values, averaging approximately 88.45%, in shapes generated by SATO, showcasing the method's strength in enhancing structural performance while maintaining visual appearance and highlighting SATO's robustness. Additionally, Fig. 5 (volfrac 45%) showed that SAGNet's material distribution was suboptimal, especially in the seat and leg regions. In contrast, SATO effectively optimized material placement in critical load-bearing areas, leading to structurally sound designs.

Overall, the results demonstrate that SATO outperforms in generating 3D shapes to achieve optimized material distribution and reduced compliance values, which marks a significant advancement over existing methods, positioning it as a robust framework for generating both visually appealing and structurally sound designs.

6.1.2. Intermediate shape interpolation in latent space

The VAE's latent space enables smooth interpolation between shapes by embedding both geometric and structural information in a continuous, low-dimensional space. Moving linearly between latent vectors of two different shapes in our SATO framework creates intermediate visually appealing and structurally sound shapes. Its performance is tested against those of SDMNet. We specifically integrated SDMNet into the interpolation section to demonstrate broader applicability.

In the test, we first generated two shapes as source and target using SDMNet and then interpolated 100 shapes between the source and target (chair), displaying shapes at specific intervals (1st, 20th, 50th, 70th, and 100th). We then input the same SDMNet-generated source and target shapes into the SATO framework. Both shapes had identical BCs, with the source having a 40% volfrac and the target a 45% volfrac.

Table 2
Parameters for Case Studies: Chair, Motorbike, Guitar, and Lamp.

Input parameter	Case study			
	Chair	Motorbike	Guitar	Lamp
Mesh Size	32 × 32 × 32	45 × 45 × 55	45 × 45 × 55	45 × 45 × 55
Volfrac	0.35–0.65	0.6–0.75	0.35–0.55	0.35–0.45
Load size (N)	10–50	20–50	10–30	5–15
Load cases	Backrest and seat	Seat and handlebar	Neck and body	Top and base
Boundary conditions	Fixed on legs	Fixed on wheels	Points where guitar is held	Fixed at base
Number of Iteration	56–82	51–72	48–76	38–61
Avg. Time Taken (sec)	5.72–7.2	11.21–9.2	14.35–12.03	14.27–13.44

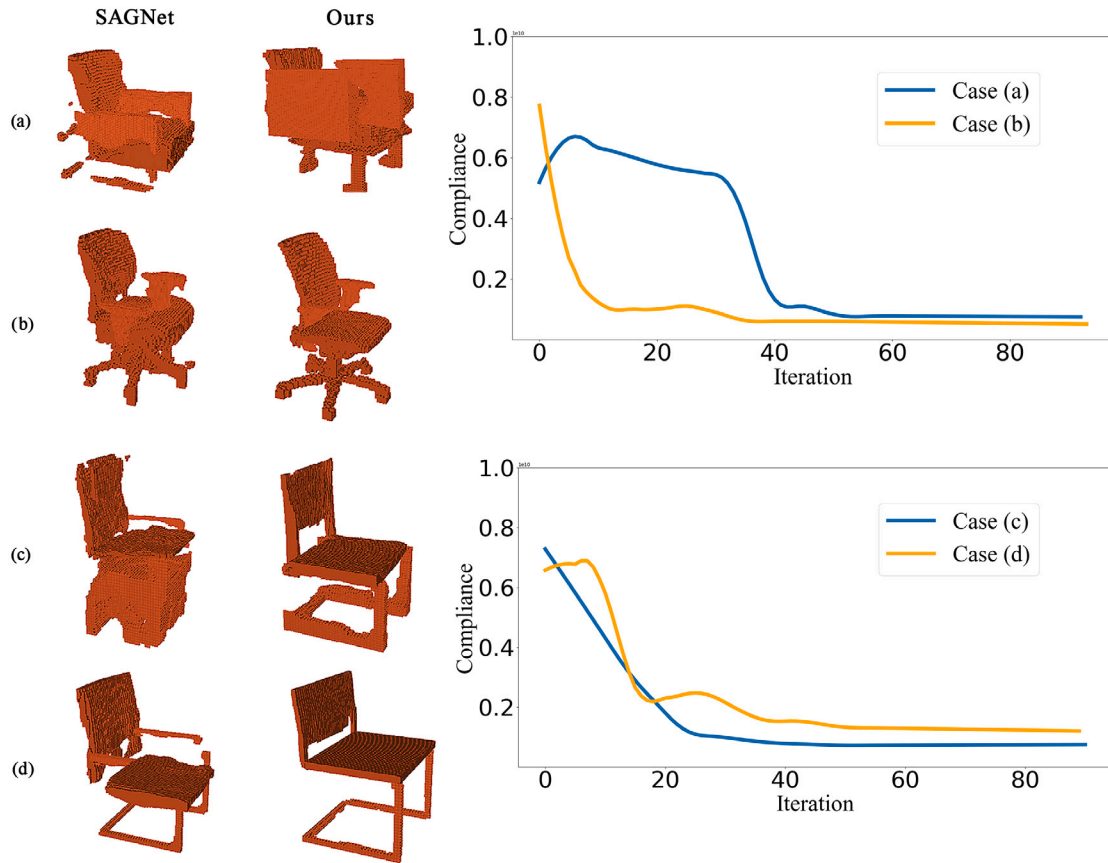


Fig. 4. Comparison between SAGNet and SATO. SAGNet’s initial decoded chair bases show suboptimal topology with irregular member sizes and connections. SATO improves these designs by setting volfrac to 45%, 40%, 35%, and 30% for a, b, c, and d, respectively. The optimized outputs (middle column) evolve into more uniform, stiffer structures.

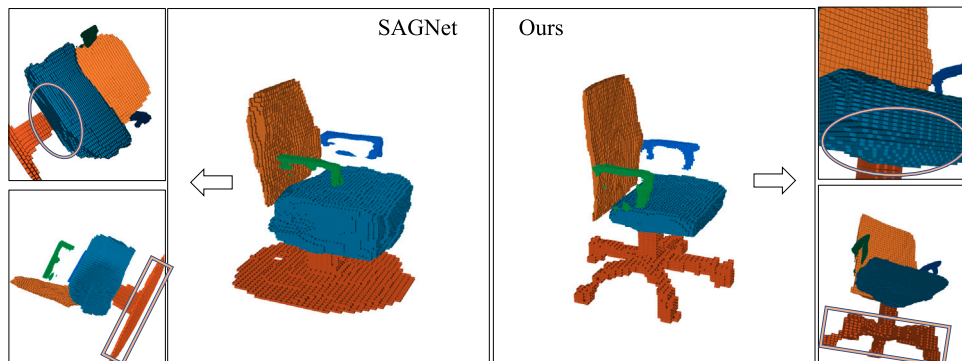


Fig. 5. Material distribution analysis. SAGNet: The leg sections are inadequately designed to withstand loading and it is overweight. SATO: our framework takes the initial shape from SAGNet, by setting volfrac as 45%, generates lightweight shapes with optimized material distribution, ensuring reinforcement in areas subjected to loads and boundary conditions.



Fig. 6. Comparison of interpolation methods. (a) Top row: SDMNet method interpolation, (b) Bottom row: SATO’s approach, demonstrating lightweight topology optimized shapes. Source and target shapes maintain volume fractions of 40% and 45% respectively.

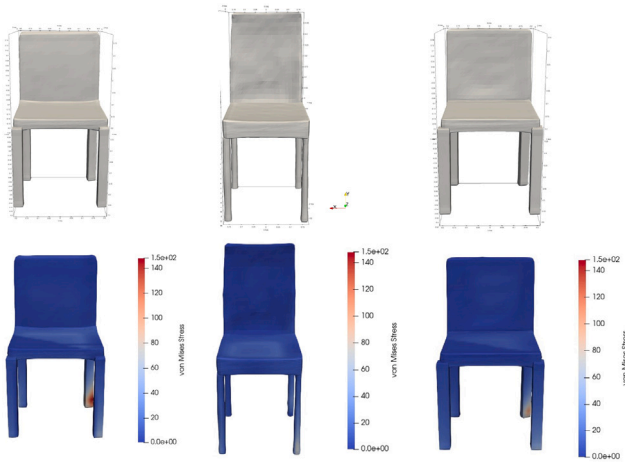


Fig. 7. Generated physically reliable shapes and their corresponding von Mises Stress distributions.

The generated shapes through SDMNet interpolation are in the top row while SATO is in the bottom row as shown in Fig. 6.

We observed that SATO produced lightweight intermediate shapes with an average reduction in compliance of 88.7% ($\pm 8.2\%$) across the interpolation sequence (Fig. 6). SATO effectively redistributed material to reinforce critical areas while maintaining the original visual appearance. The FE analysis results in Fig. 7 on the random intermediate interpolation shapes also indicate a reliable physical property of smooth stress distributions. Moreover, the FEA stress analysis is performed on the original density distribution, ensuring accurate stress calculations. The results tell that integrating TO produces intermediate shapes with improved stiffness and volume control, ensuring practical, versatile, and structurally reliable 3D shapes suitable for fast shape generation tasks.

6.2. Styled shape generation at different BCs

In the context of SATO’s work, style refers to unique variations in the structural and geometric features of generated shapes distinct from the original input. Technically, these stylistic aspect is related to the learned patterns of component configurations derived from the training data. We first test SATO’s ability in styled shape generation controlled through its BCs: varying loads and adjusting the fixed regions (Fig. 9), from a single input.

In the test, we set the volfrac as 0.45, 0.55, and 0.46 for the cases from top to bottom in Fig. 8 and default parameters mentioned in Section 6. We observed styled shape generations ranging from robust, disc-leg structures to lightweight, swivel-chair, and four-legs-chair forms. SATO is able to control material allocation and overall density, influencing the weight and form of the generated style. These transformations evolve iteratively, as seen in the convergence curves of compliance and volume (Fig. 8). The generated styles exhibit varied topology and structural designs while retaining functionality and visual quality. This showcases the dynamic nature of SATO in shape generation process and its capacity to produce stylistic and structurally sound designs.

6.3. Styled shape generation with different design settings

We further test SATO’s ability in styled shape generation controlled through design settings: different initial TO values, and different volfrac (Fig. 10). The input parameters are listed in Table 2. The six different generated shapes are shown in Fig. 10, where each column has the same initial value but a different volfrac. The optimization process typically converged within 60–90 iterations, with each iteration taking approximately 6–7.5 s, demonstrating computational efficiency.

Our approach was also tested at different volfrac for diverse case studies, including a motorbike, a guitar, and a lamp, and it successfully generated physically reliable and geometrically plausible 3D shapes (Fig. 11).

We observed that volfrac values below 0.25 lead to structural deficiencies, inadequate load support, and reduced reliability, as seen in Fig. 12. The limitations, inherent in TO, also appeared in the VAE-based TO, and we aim to address them in future work.

7. Conclusion, limitations, and future work

In the present work, a novel structure-aware topology optimization (SATO) approach is proposed. This approach overcomes the limitations of traditional approaches by incorporating geometry and corresponding structural information in a unified latent space to create mechanically robust and geometrically plausible structures. By leveraging a variational autoencoder’s latent space, we enable the generation of diverse, physically reliable designs with various styles. Numerical examples demonstrate up to 95.7% reduction in compliance, showcasing significant improvements in stiffness and stress performance. This approach bridges the gap between generative design and physics-based optimization, offering a powerful tool for creating high-performance, stylistic structures. Our method’s ability to freely interpolate between source

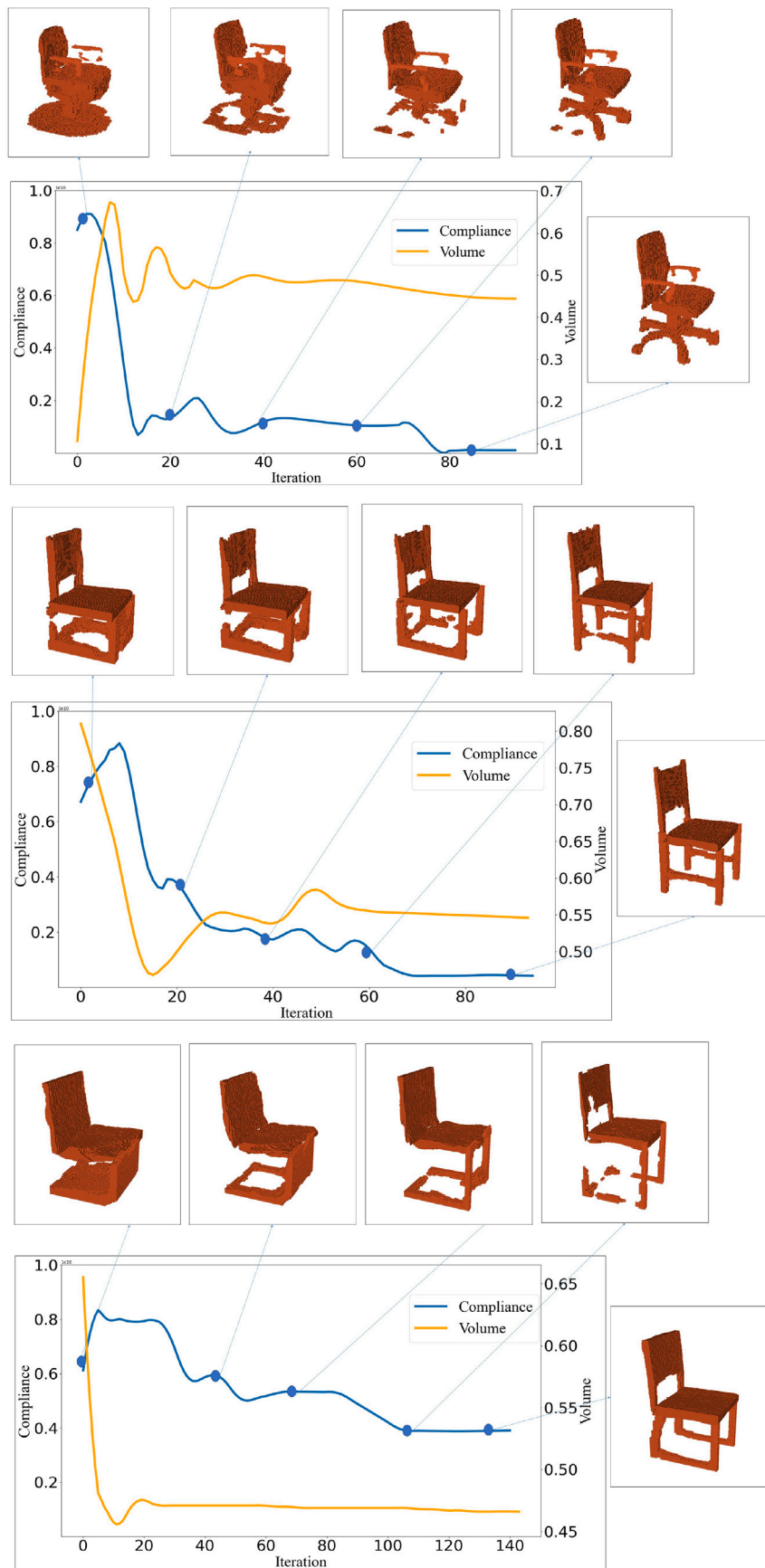


Fig. 8. Convergence curves of compliance and volume for different styles of generation, distinct from the input, along with interim results.

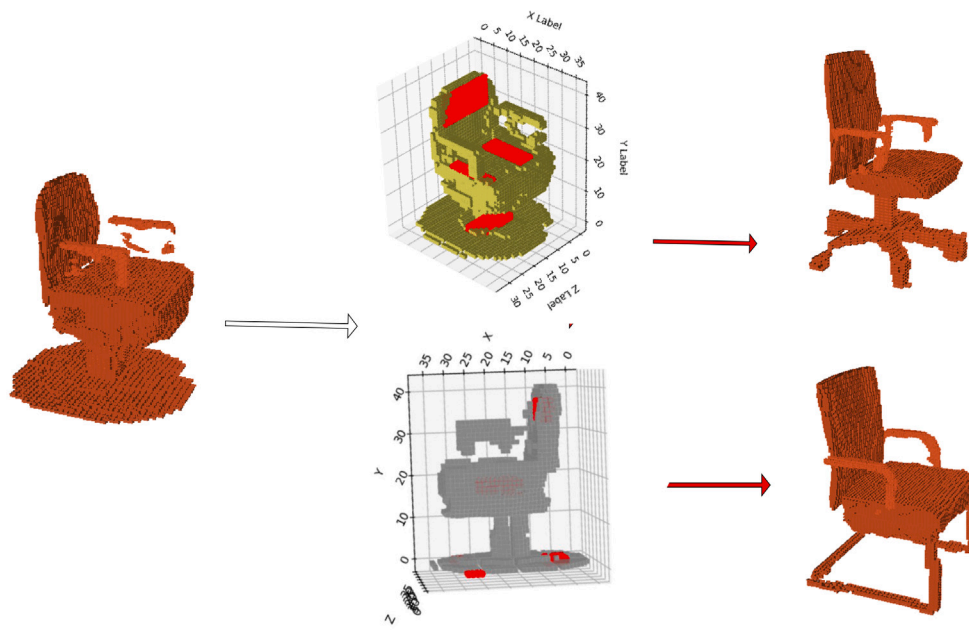


Fig. 9. Test SATO's ability in styled shape generation at different BCS. Given the same input at the left, different loads and support setups are described in the middle, and different shapes are generated at the right. Here, loads are applied to the back and seat areas of the chair (highlighted in red), while the legs serve as the fixed regions for support.

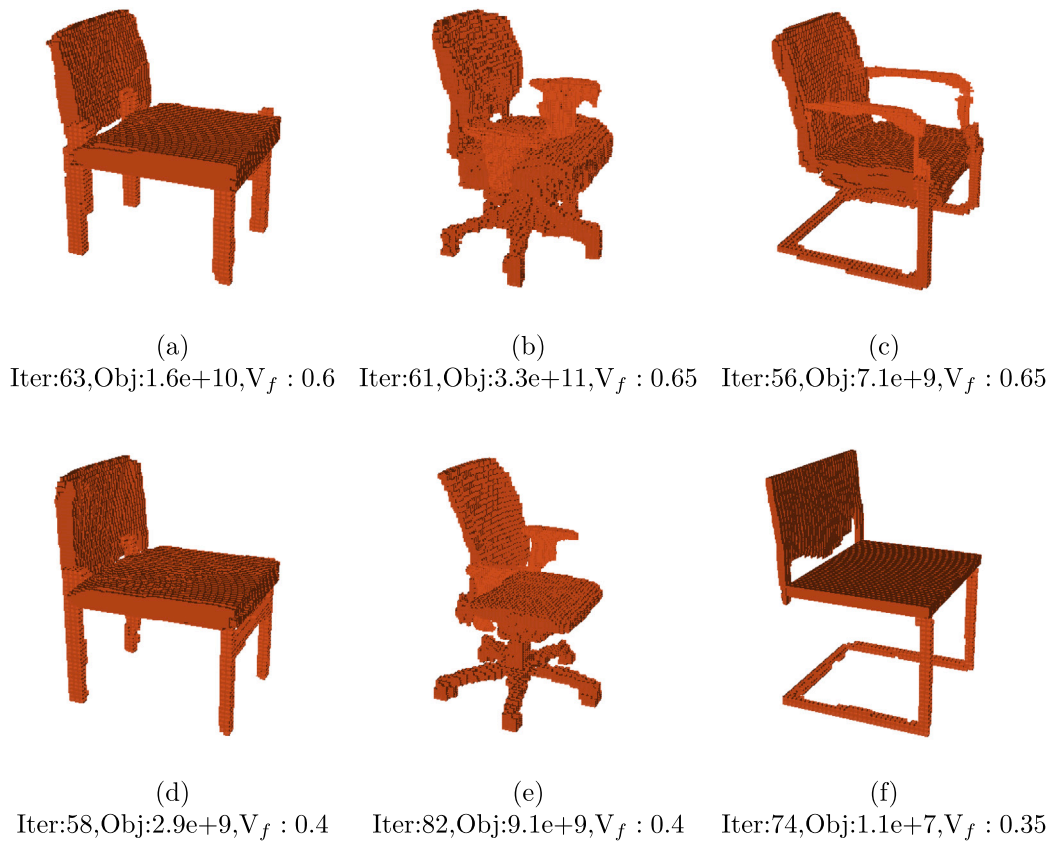


Fig. 10. Test SATO's ability in styled shape generation at various design settings: different initial TO values, and different volume fraction. Each column has the same initial values but at different volume fractions.

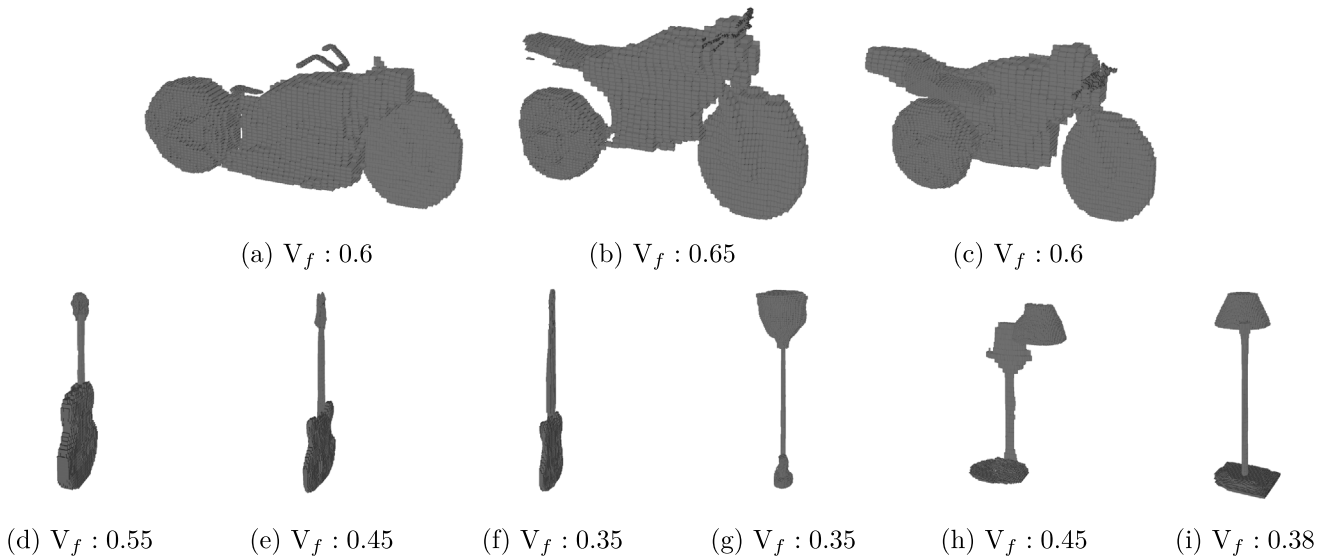


Fig. 11. Other case studies with their corresponding volume fractions shown below.



Fig. 12. The failure examples of SATO's approach when the volume fraction becomes less than 0.25.

and target shapes in latent space opens new possibilities for AI-driven design and engineering, providing a flexible and efficient solution for structural optimization with semantic control.

7.1. Limitations

Despite the promising results, the proposed approach has certain limitations that need to be addressed. Our method at present considers only volfrac as a constraint, which, while common, restricts control over the shape-generation process. For instance, the inability to incorporate user-defined constraints, such as sketch-based guidance or image-based priors [12,54], limits the flexibility and creativity of the generated shapes. Introducing such constraints could significantly enhance the method's ability to produce more diverse and user-specific designs.

Another significant limitation is the need for manual intervention to pre-set boundary conditions (BCs). This requirement not only increases the complexity of the workflow but also reduces the overall scalability of the method, particularly for large-scale or complex structures. While

concepts like simulation intent [55] or XVoxel [38] offer potential solutions by automating or simplifying the specification of BCs, integrating these approaches into our framework remains an open challenge. Addressing these limitations could produce a more robust and versatile 3D shape generation framework.

7.2. Future work

Several directions could be explored to further improve and extend the proposed approach. One promising avenue is embedding SATO within a gradient-free topology optimization (TO) framework [56–58]. This would eliminate the need for problem-specific sensitivity analysis, as discussed in Section 4.3, thereby broadening its applicability to complex industrial design problems. However, this approach comes with significant computational costs, requiring several orders of magnitude more structure simulations than gradient-based optimizers to reach convergence [58]. The integration of physics-informed neural networks (PINNs) [59] could help alleviate this issue by accelerating convergence and improving optimization efficiency.

Another key direction is the development of a surrogate deep-learning-based prediction model [59], which could significantly reduce finite element (FE) computation costs and accelerate the TO process. This enhancement would enable the method to handle more complex geometries and multi-field simulations, making it suitable for industrial applications such as automotive and consumer electronics design.

Additionally, integrating a geometry-physical coupled latent space that encodes both the physical performance and geometric attributes of a shape would be highly desirable. This would enable a fully automated, responsive design process, allowing the generation of structurally optimized and aesthetically refined models. Such advancements could enhance applications in engineering, architecture, and product design, further bridging the gap between AI-driven generative design and physics-based optimization.

CRedit authorship contribution statement

Haroon Ijaz: Writing – original draft, Software, Methodology. **Xuwei Wang:** Writing – review & editing, Methodology, Investigation. **Wei Chen:** Writing – original draft, Visualization, Validation. **Hai Lin:** Project administration, Conceptualization. **Ming Li:** Writing – review & editing, Supervision, Resources, Methodology, Funding acquisition, Conceptualization.

Declaration of competing interest

The authors declare that they have no known competing financial interests or personal relationships that could have appeared to influence the work reported in this paper.

Acknowledgments

We would like to thank all the anonymous reviewers for their valuable comments and suggestions. The work described in this paper is partially supported by the National Key Research and Development Program of China (No. 2020YFC2201302) and the NSF of China (No. 62372401).

Data availability

Data will be made available on request.

References

- [1] Regenwetter L, Nobari AH, Ahmed F. Deep generative models in engineering design: A review. 2021, arXiv abs/2110.10863.
- [2] Bendsoe MP, Sigmund O. Topology optimization: theory, methods, and applications. 2013.
- [3] Sutradhar A, Park J, Haghghi P, Kresslein J, Detwiler D, Shah JJ. Incorporating manufacturing constraints in topology optimization methods: A survey. 2017.
- [4] Zhang W, Tian H, Sun Z, Feng W. Topology optimization for pressure loading using the boundary element-based moving morphable void approach. *Adv Eng Softw* 2024;195:103689.
- [5] Hu J, Li M, Gao S. Texture-guided generative structural designs under local control. *Comput- Aided Des* 2019;108:1–11.
- [6] Yang D, Liu H, Zhang W, Li S. Stress-constrained topology optimization based on maximum stress measures. *Comput Struct* 2018;198:23–39.
- [7] Guan Y, van Kaick O. Diverse part synthesis for 3D shape creation. *Comput-Aided Des* 2024;175:103746.
- [8] Wu Z, Wang X, Lin D, Lischinski D, Cohen-Or D, Huang H. SAG-Net: Structure-aware generative network for 3D-shape modeling. *ACM Trans Graph* 2018;38:1–14.
- [9] Huang X, Li S, Zhang S, Hao A, Qin H. Distribution-motivated 3D style characterization based on latent feature decomposition. *Comput- Aided Des* 2022;153:103399.
- [10] Gao L, Yang J, Wu T, Yuan Y-J, Fu H, Lai Y-K, et al. SDMNet: Deep generative network for structured deformable mesh. *ACM Trans Graph* 2019;38(6):243:1–243:15.
- [11] Kingma DP, Welling M. Auto-encoding variational bayes. 2013, arXiv preprint arXiv:1312.6114.
- [12] Mittal P, Cheng Y-C, Singh M, Tulsiani S. Autosdf: Shape priors for 3d completion, reconstruction and generation. In: Proceedings of the IEEE/CVF conference on computer vision and pattern recognition. 2022, p. 306–15.
- [13] Xie H, Yao H, Sun X, Zhou S, Zhang S. Pix2vox: Context-aware 3d reconstruction from single and multi-view images. In: Proceedings of the IEEE/CVF international conference on computer vision. 2019, p. 2690–8.
- [14] Mo K, Guerrero P, Yi L, Su H, Wonka P, Mitra N, et al. StructureNet: Hierarchical graph networks for 3D shape generation. *ACM Trans Graph* 2019;38(6):242.
- [15] Melas-Kyriazi L, Ruppel C, Vedaldi A. PC2: Projection-conditioned point cloud diffusion for single-image 3D reconstruction. In: Proceedings of the IEEE/CVF conference on computer vision and pattern recognition. 2023, p. 12923–32.
- [16] Zhou L, Du Y, Wu J. 3D shape generation and completion through point-voxel diffusion. In: Proceedings of the IEEE/CVF international conference on computer vision. 2021, p. 5826–35.
- [17] Sella E, Fiebelman G, Hedman P, Averbuch-Elor H. Vox-e: Text-guided voxel editing of 3d objects. In: Proceedings of the IEEE/CVF international conference on computer vision. 2023, p. 430–40.
- [18] Wang X, Ang MH, Lee GH. Voxel-based network for shape completion by leveraging edge generation. In: Proceedings of the IEEE/CVF international conference on computer vision. 2021, p. 13189–98.
- [19] Liu J, Huang X, Huang T, Chen L, Hou Y, Tang S, et al. A comprehensive survey on 3D content generation. 2024, arXiv abs/2402.01166.
- [20] Li X, Xie C, Sha Z. Design representation for performance evaluation of 3D shapes in structure-aware generative design. *Des Sci* 2023;9:e27.
- [21] Wen C, Zhang Y, Cao C, Li Z, Xue X, Fu Y. Pixel2Mesh++: 3D mesh generation and refinement from multi-view images. *IEEE Trans Pattern Anal Mach Intell* 2022;45(2):2166–80.
- [22] Cheng Y-C, Lee H-Y, Tulyakov S, Schwing AG, Gui L. SDFusion: Multimodal 3D shape completion, reconstruction, and generation. In: 2023 IEEE/CVF conference on computer vision and pattern recognition. 2022, p. 4456–65.
- [23] Zhang B, Tang J, Niessner M, Wonka P. 3Dshape2vecset: A 3d shape representation for neural fields and generative diffusion models. *ACM Trans Graph* 2023;42(4):1–16.
- [24] Zhao Z, Liu W, Chen X, Zeng X, Wang R, Cheng P, et al. Michelangelo: Conditional 3d shape generation based on shape-image-text aligned latent representation. *Adv Neural Inf Process Syst* 2024;36.
- [25] Yariv L, Gu J, Kasten Y, Lipman Y. Volume rendering of neural implicit surfaces. *Adv Neural Inf Process Syst* 2021;34:4805–15.
- [26] Yin F, Liu W, Huang Z, Cheng P, Chen T, Yu G. Coordinates are not lonely-codebook prior helps implicit neural 3d representations. *Adv Neural Inf Process Syst* 2022;35:12705–17.
- [27] Cheng Y-C, Lee H-Y, Tulyakov S, Schwing A, Gui L. SDFusion: Multimodal 3D shape completion, reconstruction, and generation. In: CVPR. 2023.
- [28] Zhao Z, Liu W, Chen X, Zeng X, Wang R, Cheng P, et al. Michelangelo: Conditional 3D shape generation based on shape-image-text aligned latent representation. 2023, arXiv preprint arXiv:2306.17115.
- [29] Yin F, Chen X, Zhang C, Jiang B, Zhao Z, Fan J, et al. Shapepnt: 3d shape generation with a unified multi-modal language model. 2023, arXiv preprint arXiv:2311.17618.
- [30] Sanghi A, Chu H, Lambourne JG, Wang Y, Cheng C-Y, Fumero M, et al. Clip-forge: Towards zero-shot text-to-shape generation. In: Proceedings of the IEEE/CVF conference on computer vision and pattern recognition. 2022, p. 18603–13.
- [31] Xu Q-C, Mu T-J, Yang Y-L. A survey of deep learning-based 3D shape generation. *Comput Vis Media* 2023;9:407–42.
- [32] Asperti A, Evangelista D, Piccolomini EL. A survey on variational autoencoders from a green AI perspective. *SN Comput Sci* 2021;2.
- [33] Park JJ, Florence P, Straub J, Newcombe R, Lovegrove S. DeepSDF: Learning continuous signed distance functions for shape representation. In: Proceedings of the IEEE/CVF conference on computer vision and pattern recognition. 2019, p. 165–74.
- [34] Chen J, Shapiro V, Suresh K, Tsukanov I. Shape optimization with topological changes and parametric control. *Internat J Numer Methods Engrg* 2007;71(3):313–46.
- [35] Liu J, To AC. CAD-based topology optimization system with dynamic feature shape and modeling history evolution. *J Mech Des* 2019;142(7):1–25.
- [36] Hafner C, Schumacher C, Knoop E, Auzinger T, Beyer M. X-CAD: optimizing CAD models with extended finite elements. *ACM Trans Graph* 2019;38(6):1–15.
- [37] Zhou Y, Zhang W, Zhu J, Xu Z. Feature-driven topology optimization method with signed distance function. *Comput Methods Appl Mech Engrg* 2016;310:1–32.
- [38] Li M, Lin C, Chen W, Liu Y, Gao S, Zou Q. XVoxel-based parametric design optimization of feature models. *Comput- Aided Des* 2023;160:103528.
- [39] Guo X, Zhang W, Zhong W. Doing topology optimization explicitly and geometrically—A new moving morphable components based framework. *J Appl Mech* 2014;81(8):081009.
- [40] Zhang W, Yuan J, Zhang J, Guo X. A new topology optimization approach based on Moving Morphable Components (MMC) and the ersatz material model. *Struct Multidiscip Optim* 2016;53:1243–60.

- [41] Zhang W, Li D, Zhang J, Guo X. Minimum length scale control in structural topology optimization based on the Moving Morphable Components (MMC) approach. *Comput Methods Appl Mech Engrg* 2016;311:327–55.
- [42] Shin SC, Shin D, Kang N. Topology optimization via machine learning and deep learning: A review. 2022, arXiv abs/2210.10782.
- [43] Zhang W, Wang Y, Du Z, Liu C, Youn S-K, Guo X. Machine-learning assisted topology optimization for architectural design with artistic flavor. *Comput Methods Appl Mech Engrg* 2023;413:116041.
- [44] Erva Ulu RZ, Kara LB. A data-driven investigation and estimation of optimal topologies under variable loading configurations. *Comput Methods Biomech Biomed Eng.: Imaging Vis* 2016;4(2):61–72.
- [45] Abueidda DW, Koric S, Sobh NA. Topology optimization of 2D structures with nonlinearities using deep learning. *Comput Struct* 2020;237:106283.
- [46] Jeong H, Batuwatta-Gamage C, Bai J, Xie YM, Rathnayaka C, Zhou Y, et al. A complete Physics-Informed Neural Network-based framework for structural topology optimization. *Comput Methods Appl Mech Engrg* 2023;417:116401.
- [47] Zhang W, Yang Z, Jiang H, Nigam S, Yamakawa S, Furuhashi T, et al. 3D shape synthesis for conceptual design and optimization using variational autoencoders. 2019, arXiv:1904.07964.
- [48] Wu Z, Song S, Khosla A, Yu F, Zhang L, Tang X, et al. 3D ShapeNets: A deep representation for volumetric shapes. In: 2015 IEEE conference on computer vision and pattern recognition. 2015, p. 1912–20.
- [49] Guo T, Lohan DJ, Allison JT, Cang R, Ren Y. An indirect design representation for topology optimization using variational autoencoder and style transfer. In: 2018 AIAA/aSCE/AHS/aSC structures, structural dynamics, and materials conference. 2018, p. 0804.
- [50] Svanberg K. MMA and GCMMA-two methods for nonlinear optimization. vol. 1, 2007, p. 1–15.
- [51] Chung J, Gülçehre Ç, Cho K, Bengio Y. Empirical evaluation of gated recurrent neural networks on sequence modeling. 2014, arXiv abs/412.3555.
- [52] Deng H, Saitou K. A novel discrete adjoint-based level set topology optimization method in B-spline space. *Optim Eng* 2024;25(3):1505–30.
- [53] Allaire G. A review of adjoint methods for sensitivity analysis, uncertainty quantification and optimization in numerical codes. *Ingénieurs de L'Automob* 2015;836:33–6.
- [54] Binninger A, Hertz A, Sorkine-Hornung O, Cohen-Or D, Giryès R. SENS: Part-aware sketch-based implicit neural shape modeling. *Comput Graph Forum* 2023;43.
- [55] Boussuge F, Tierney CM, Vilmart H, Robinson TT, Armstrong CG, Nolan DC, et al. Capturing simulation intent in an ontology: CAD and CAE integration application. *J Eng Des* 2019;30(10–12):688–725.
- [56] Papadrakakis M, Lagaros ND, Tsompanakis Y. Structural optimization using evolution strategies and neural networks. *Comput Methods Appl Mech Engrg* 1998;156(1):309–33.
- [57] Guirguis D, Coello CAC, Saitou K, Aulig N, Picelli R, Zhu B, et al. Evolutionary black-box topology optimization: Challenges and promises. *IEEE Trans Evol Comput* 2020;24:613–33.
- [58] Kuš G, Bessa MA. Gradient-free neural topology optimization. 2024, arXiv abs/2403.04937.
- [59] Raissi M, Perdikaris P, Karniadakis G. Physics-informed neural networks: A deep learning framework for solving forward and inverse problems involving nonlinear partial differential equations. *J Comput Phys* 2019;378:686–707.